



Experimental study on the failure process of water-bearing rock under uniaxial tension based on dominant frequency analysis of acoustic emission

Jun Zhu^{1,2} · Jianhui Deng² · Ronald Y. S. Pak³ · Jianfeng Liu² · Cheng Lyu²

Received: 7 October 2022 / Accepted: 2 April 2023 / Published online: 29 May 2023
© Springer-Verlag GmbH Germany, part of Springer Nature 2023

Abstract

Water has substantial effects on the tensile failure behavior of rock engineering materials in excavations and underground openings. However, our understanding of the tensile failure process of wet rock and its water-weakening mechanism is limited. In this sense, a series of uniaxial tension tests, coupled with acoustic emission (AE) signal monitoring, were carried out on dry, natural, and saturated marble rock. Importantly, the dominant frequencies of AE waveforms recorded during the tension loading were analyzed by a newly introduced quantitative statistical method. The test results show that the increasing water content of marble rock leads to significant strength reductions while having no relation with the twin-peak feature of dominant frequency bands of AE waveforms. The statistical analysis suggests that the dominant micro-tensile failures always appear before micro-shear failures and increase slightly with an increase in water content. The weak pore water pressure causes the initial release moments of micro-tensile failures for natural and saturated rocks to be advanced. With increasing water contents, more micro-tensile failures carrying less energy occur, while the amount and energy of micro-shear failure both reduce significantly. The mechanism involved in the drastic tensile strength reduction is likely to be friction weakening because of the water films, which is manifested by a significant loss in the amount and energy of micro-shear failures. This work provides a reasonable explanation for the tensile strength reduction of water-bearing rock by connecting the rock micro-failure and the dominant frequency of AE waveform signals released.

Keywords Water content · Tensile strength · Acoustic emission · Dominant frequency · Micro-failure

Introduction

To evaluate the stability and reliability of engineering constructions, it is essential to understand the rock tensile mechanical properties extensively (Hobbs 1967; Liao et al. 2019). Tensile stress occurs widely in many rock engineering

applications such as rock caverns, rock slopes, and rock foundations subject to vibration or earthquake. In reality, the process of rock brittle fracture usually is a tensile failure process, which results in the failure of rock slope, splitting, spalling, and rock bursting in deep excavation. Moreover, as the macro-deformation and fracture of rock mass essentially originate from nucleation, propagation, and accumulation of micro-tensile failure, it is thus of immense concern to investigate the micro-failure process of rock under tension.

Water is one of the important factors affecting the deformation and failure behavior of rock under not only compression but also tension. Compared to the fruitful results under compression (Kim et al. 2017; Liu et al. 2020; Rabat et al. 2020; Shakoor and Barefield 2009), research on water-weakening effects on tensile behavior is less detailed. Over the decades, Brazilian tests (Talesnick et al. 2001; Wong and Jong 2014), point-loading tests (Gunsallus and Kulhawy 1984; Lajtai 1980), and bending tests (Van 1976) have been conducted because of their easy application. These

✉ Jun Zhu
zhujun@imde.ac.cn

¹ Key Laboratory of Mountain Hazards and Earth Surface Process, Institute of Mountain Hazards and Environment, Chinese Academy of Sciences (CAS), Chengdu 610299, China

² State Key Laboratory of Hydraulics and Mountain River Engineering, College of Water Resources and Hydropower, Sichuan University, Chengdu 610065, China

³ Department of Civil, Environmental and Architectural Engineering, University of Colorado, Boulder, CO 80309, USA

experimental studies reported that tensile strengths are lower in wet compared with dry conditions, and its reduction depends on the rock type. However, there is a difference between the tensile strength of the rock in direct and indirect tension tests (Liu et al. 2014; Perras and Diederichs 2014). Even though a few direct tension experiments were conducted and proposed the uniaxial tensile strength reduction of saturated rocks (Hashiba and Fukui 2015; Ojo and Brook 1990), the study on direct tensile behavior, especially for its micro-failure process, is far from though. In particular, the underlying micro-failure process of rock under different water contents was seldom investigated and its water content effects were typically not reported and discussed. To our best knowledge, this dilemma is mainly due to two insufficient aspects.

The first is the realization of the pure tensile uniaxial stress state. In the uniaxial tension test, it is assumed that the stress state is truly uniform and uniaxial, and the tensile strength can thus be computed as the ratio of the rupture force and the area of the specimen cross-section. Unfortunately, these assumptions are rarely valid because the primary defects and stress concentrations at the specimen grips can be responsible for an early failure of the specimen. Hence, monitoring the micro-failure process of rock under uniaxial tension becomes challenging. The second is the presence of multiple water-weakening factors. Similar to wet rock under compression, there are various potential water-weakening effects, e.g., pore water pressure, friction weakening, and stress corrosion, of rock under tension (Zhu et al. 2022). In particular, these water-weakening effects are often exerted at the same time, which causes tensile mechanical degradation. As a result, the contribution of one specific water-weakening effect is ambiguous and it is still rather a challenge to evaluate the failure process of wet rock under uniaxial tension.

Acoustic emissions signals (AEs) are defined as the transient elastic wave associated with a rapid release of localized strain energy reflecting the micro-failure characteristics within a material (Calabrese et al. 2013; Lockner 1993). It has been proven to be a useful tool for analyzing the real-time activities of micro-failure of rock subjected to an external load (Aker et al. 2014; Liu et al. 2015; Ohnaka and Mogi 1982). Based on the detected AE signals, the AE characteristic such as AE signal parameters (i.e., count, rising time, amplitude, and energy) of AE events can be analyzed (Li et al. 2020; Zhang et al. 2018). These AE characteristics parameters could be easily evaluated and further advance our understanding of the crack propagation and failure behavior of moisture rocks. For example, Eberhardt et al. (1998) and Yao et al. (2016) evaluated the crack initiation stress threshold of saturated rocks by AE parameters, e.g., AE counts and AE hits. Sun et al. (2016) studied the burst feature of water-bearing sandstone and reported that

the AE cumulative counts of saturated sandstone released during the tests reduced when compared to dry sandstone. The AE events reductions of rocks after saturation were also found in the research conducted by Verstrynge et al. (2014) and Vishal et al. (2015). Zhao et al. (2021) analyzed the AE amplitude-frequency characteristics and further investigate the micro-cracking behavior of red sandstone under different water contents. Wang et al. (2021) reported that the joints and water both affect the AE parameters of signals captured during shear loading tests.

In contrast to the AE parameters analysis, the AE waveform-based analysis is time-consuming under the premise of the high precision of the equipment. Despite its shortcomings, the waveform-based analysis is considered worthwhile because AE waveform signals carry the intrinsic information of rock failure. Thanks to the development of AE sensors and computational processors, the dominant frequencies of AE waveforms were extracted in batches and used to study the micro-failure process of rock (He et al. 2010; Shiotani et al. 2001; Zhang and Deng 2020). Chugh et al. (1968) concluded that the dominant frequencies of AE waveforms collected in the tension tests of sandstone, limestone, and granite are mostly located in the ranges of 0–6 kHz and 10–15 kHz. Zhang et al. (2015) analyzed the AE characteristics of dry and saturated coal gangue under compression and found that the dominant frequencies of AE waveforms are mainly distributed around 20 kHz and in the range of 30–60 kHz. Furthermore, Li et al. (2017) and Li (2017) proposed that there are two dominant frequency concentration bands, which were verified by numerous tests in different rocks under different loading regimes. According to the first motion polarity method and the moment tensor method proposed by Zang et al. (1998), Ohtsu (1991), and Ohtsu et al. (1998), these researchers also validated the AE waveforms distributed in high dominant frequency bands are produced by micro-shear failure and the AE waveforms located in low dominant frequency bands are released by micro-tensile failure. It should be noted that the variables of the aforementioned studies are rock integrity, i.e., intact and jointed rocks, and loading regimes, i.e., compression, shear, and Brazilian. The study on the tensile failure of rock under different water contents using statistical analysis of AE waveforms, however, is still in its infancy to date. In this connection, the statistical analysis of AE dominant frequency may provide a new way to evaluate the rock failure process quantitatively.

The abovementioned points indicate that the theory gap of the failure process and underlying water-weakening mechanisms of rock under different water contents is expected to be filled by the new AE waveform statistical analysis method. In this work, marble rock with single mineral composition was selected to distinguish multiple potential water-weakening effects. The specific objectives of this work are firstly, to quantify the water content effects on tensile

mechanical properties (i.e., tensile strength and modulus) of marble rock; secondly, to describe the tensile failure process of rock under different water contents quantitatively by the new introduced statistical analysis of the dominant frequencies of AE waveforms; and thirdly, to propose the water-weakening mechanisms responsible for tensile strength degradation based on statistical analysis results.

Experimental process

Specimen preparation

White marble was collected in Baoxing County, Sichuan Province, China. The mineralogical composition was determined by X-ray single-crystal diffractometer (XRD) analysis, showing only a single mineral, namely, calcite (see Fig. 1a). The thin-section image of marble under cross-polarized light (XPL) emphasizes its dense structure, as well as slight fissured, as shown in Fig. 1b. According to the standard of the International Society for Rock Mechanics and Rock Engineering (Culshaw 2015), all cylindrical samples were prepared with a $\sim 2L/D$ ratio for uniaxial tension tests (length: ~ 100 mm, diameter: ~ 50 mm). The two end faces were ground to ensure that both planes were parallel with an accuracy of ± 0.05 mm and perpendicular to the longitudinal

axis with an accuracy of $\pm 0.25^\circ$. Especially, a circumferential surface pre-crack with 2 mm in width and 3 mm in depth was made in the middle of each sample. Note that, this artificial pre-crack has a slight impact on the tensile strength of the rock, but guarantees the consistency of fracture modes, which is conducive to the AE analysis in the following (Li et al. 2017; Wang et al. 2019). The porosity value of marble was approximately 8.32%. The density value under natural conditions was around $2.67 \text{ g}\cdot\text{cm}^{-3}$. The velocity of the P-wave was about 3217 m/s.

Samples under the dry condition for testing group 1, consisting of TMD-1, TMD-2, TMD-4, and TMD-5, and under the natural condition for testing group 2, consisting of TMN-1 ~ TMN-4, and under the saturated condition for testing group 3, consisting of TMS-1 ~ TMS-4, were obtained by different methods explained as follows in detail.

- (1). Samples of group 1 were dried in an oven at 105°C for 48 h and cooled to room temperature. A high-strength adhesive, JGN, was used to bond the tensile loading slider to the samples, and it reaches its maximum strength within 3~5 days. During the entire process, samples and sliders are placed in a dry box to avoid the effects of environmental humidity.
- (2). Samples of group 2 were bonded with sliders directly. After 3~5 days, samples with sliders are exposed to indoor air.
- (3). Samples of group 3 were dried first and then bonded with sliders. After the maximum strength of adhesive reaches, samples with sliders were all soaked in water for more than 48 h and stood for 4 h to achieve saturated conditions. Each Sample was blotted with a moist cloth before the test. As shown in Fig. 2, the water content of TMS-1 was calculated by an increase in sample mass regularly and was found to keep con-

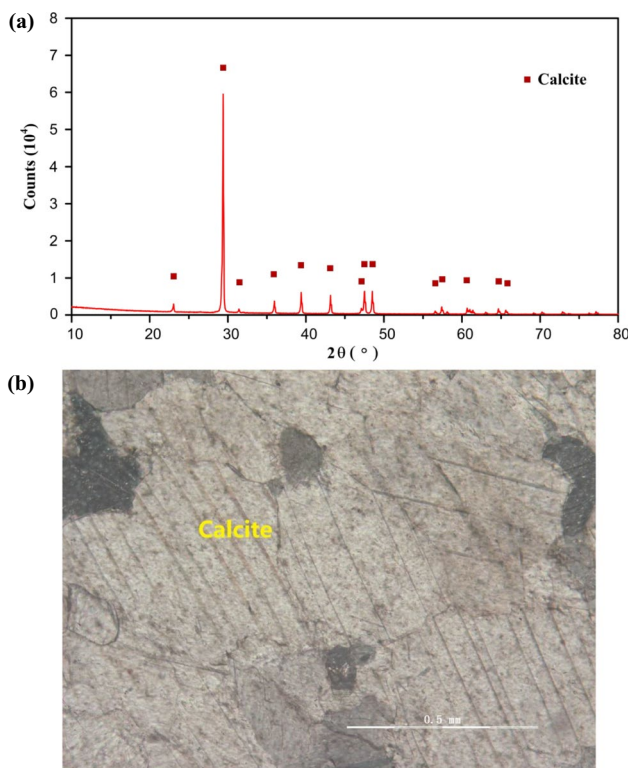


Fig. 1 The results of XRD and XPL measurement for marble rock

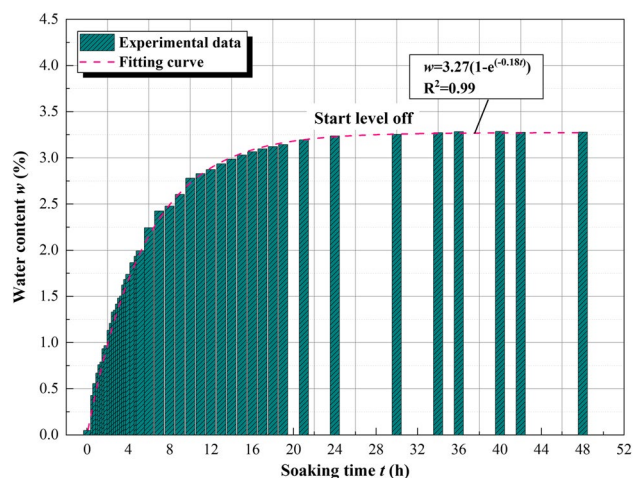


Fig. 2 Variation of water content with water soaking time

stant after soaking for 24 h. Hence, the samples of group 3 saturated in water over 48 h were believed to be fully saturated.

Experimental apparatuses and procedure

A rock mechanics test system (Model: MTS815 Flex Test GT) and AE monitoring system (Model: PCI-2) were employed to conduct uniaxial tension tests on white marble shown in Fig. 3a. The capacity of the axial load transducer was 1000 kN. A linear variable differential transformer (LVDT) with a range of ± 2.5 mm was used to measure axial displacement. The loading rate was kept constant at 0.05 mm/min. Eight micro 30 sensors were installed symmetrically in the radial direction along the surface of the cylinder to capture AE waveforms (Fig. 3). The micro 30 sensors with low resonance frequency have good sensitivity and frequency response to AE data. The sampling frequency is 1 MHz, and the pre-amplification is 40 dB. To enhance the connections between sensors and samples, Vaseline was used as a coupling agent.

Data processing

Figure 4 illustrated the extraction process of the dominant frequency of an AE waveform. All the AE waveform signals

captured during the loading application can be sorted by loading time using the batch processing function of Windows first in this study. Since the AE signals are non-stationary, the fast Fourier transformation (FFT) was then selected to transform the AE waveforms recorded into amplitude spectra with the aid of MATLAB programming. From the frequency domain, one can determine the dominant frequency (frequency corresponding to the greatest amplitude) and the amplitude of the AE waveform. Simply, the energy of one AE waveform is represented by the square of its amplitude. As a result, all dominant frequencies of AE waveforms and their amplitude can be obtained and further used to analyze the rock tensile failure process based on statistical analysis.

Experimental results and discussions

Tensile mechanical properties of water-bearing rock

We calculated the tensile strength σ_t by the ratio of maximum axial force P_{max} and the area of the middle cross-section of rock sample S . It should be noted that the tensile strength σ_t measured in this work is not the real uniaxial tensile strength in the traditional sense due to the existence of artificial pre-crack; however, the same conditions of pre-crack for dry, natural, and saturated rock samples not only

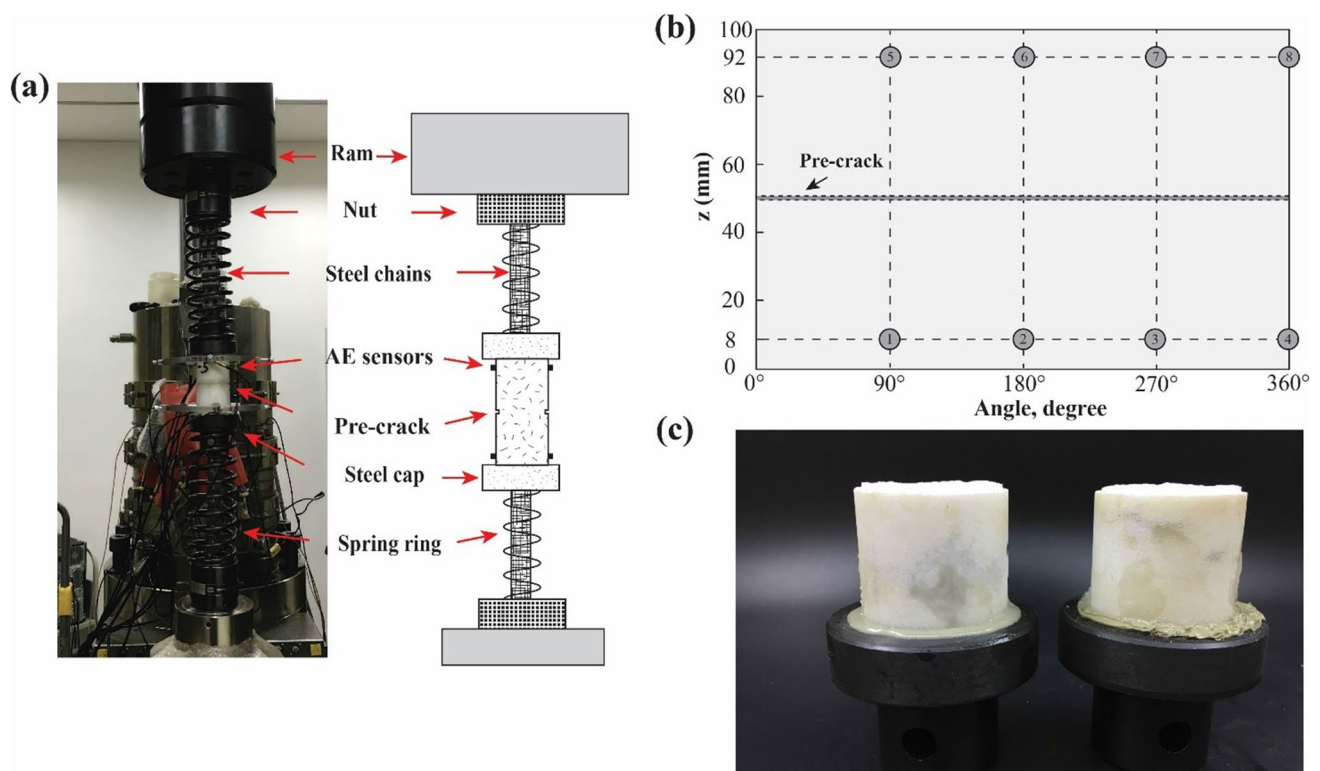
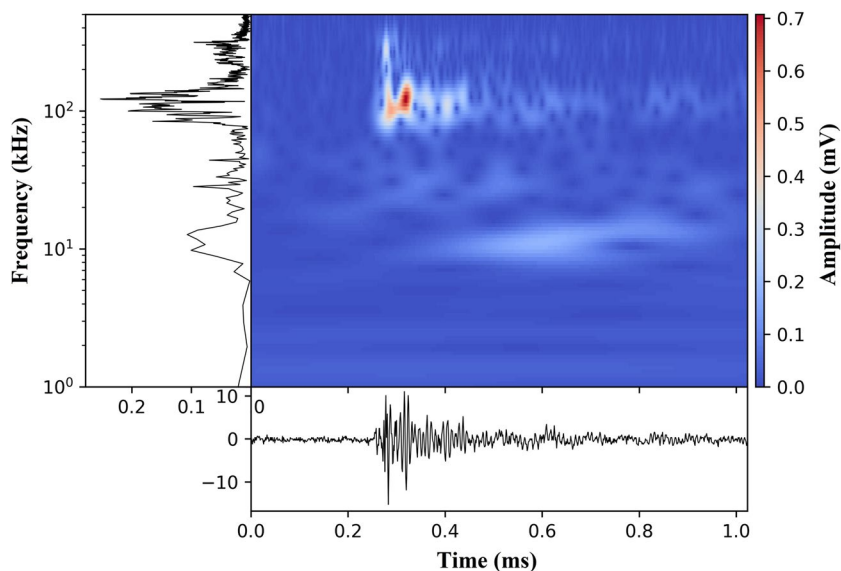


Fig. 3 Uniaxial tension tests for rock specimens, **a** experimental setup, **b** diagram of AE sensors layout, **c** rock fracture pattern

Fig. 4 Extraction process of the dominant frequency of AE waveform



have no effects on comparison analysis but also keep the fracture pattern consistent because all rock specimens are prone to fail along the artificial pre-crack (see Fig. 3c). The two equations for calculating σ_t are as follows:

$$\sigma_t = \frac{P_{max}}{S} \tag{1}$$

$$S = \pi \left(\frac{D}{2} - L \right)^2 \tag{2}$$

where D and L represent the diameter of the rock sample and the depth of the circumferential surface pre-crack.

The water content of each sample was obtained by the traditional weight difference method. The average water

content of natural and saturated samples increase to 0.96% and 3.29% compared with 0 for dry samples. It indicates that marble in its natural state has very little water, resulting in a lower increment in water content compared with saturated marble rock. In addition, the tangential modulus at 50% of peak stress was selected as the deformation modulus (Hawkes et al. 1973; Stimpson and Chen 1993). The data of tensile strength and moduli and their variation with water contents are illustrated in Table 1 and Fig. 5.

In general, the results demonstrate a significant loss of tensile strength of marble rock as a consequence of its increasing water contents. Note that, the tensile strength and modulus data of TMN-3 in group 3 was not included in the average calculation because of its great dispersion;

Table 1 Mechanical properties parameters of all samples

No	Rock condition	w (%)	σ_t (MPa)	Avg. σ_t (MPa)	E_t (Gpa)	Avg. E_t (Gpa)
TMD-1	Dry	0	2.38	2.46	3.01	3.14
TMD-2		0	2.25		2.23	
TMD-4		0	2.60		3.85	
TMD-5		0	2.62		3.47	
TMN-1		Natural	0.97		2.36	
TMN-2	0.92		2.19	3.00		
TMN-3	1.07		1.56	0.73		
TMN-4	0.86		2.21	4.16		
TMS-1	Saturated	3.28	1.76	1.75	1.82	1.98
TMS-2		3.19	1.83		2.01	
TMS-3		3.36	1.70		2.40	
TMS-4		3.31	1.71		1.69	

w (%) water content, $w = m_w/m_d \times 100$, where m_d and m_w are the mass of solid and water of rock specimen, σ_t (MPa) tensile strength, E_t (Gpa) deformation modulus, the average tensile strength, and deformation modulus for the natural group is obtained by missing TMN-3

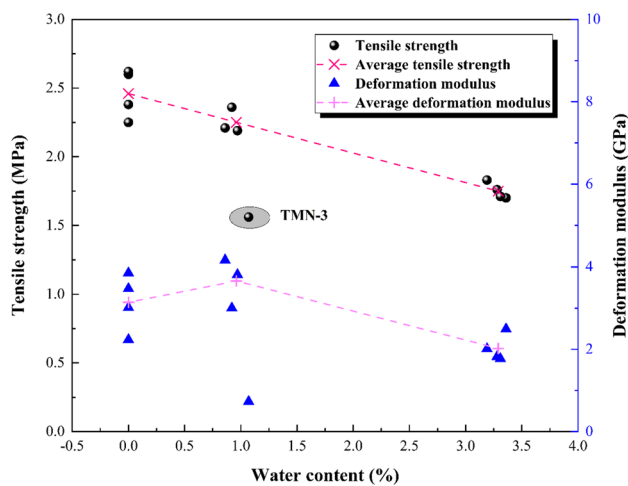


Fig. 5 Variation of tensile strength and deformation modulus versus water content. The average tensile strength and deformation modulus of the natural group were obtained by missing TMN-3

this big dissimilar behavior of TMN-3 is probably due to its heterogeneous microstructure, such as joints inside. The average tensile strength for dry and natural specimens is 2.46 and 2.25 MPa, respectively. When specimen conditions change to saturated, the average value drops significantly to 1.75 MPa, with a reduction of 28.86%. However, the deformation modulus exhibited weak correlations with water content when compared with tensile strength results. The resulting deformation moduli within a particular group show larger data scatter, especially for dry and natural groups. The average modulus for dry specimens is 3.14 GPa, while those for natural and saturated specimens are 3.66 and 1.98 GPa, respectively. Apart from the overall reduction in the average tensile strength and deformation modulus, small data variations of them are also observed due to the presence of water, which agrees with the prior experimental results proposed by Wong and Jong (2014).

Statistical analysis of the dominant frequency of AE waveforms

To statistically analyze the dominant frequency characteristic of AE waveforms, dominant frequencies were divided into 46 bands in this study. The interval of each band is 10 kHz except for the last band. Since the dominant frequencies of rock are mostly within the range of 0 to 450 kHz, dominant frequencies beyond 450 kHz are all included in the NO. 46 band. Furthermore, the dominant frequency bands whose percentage of characteristic parameters (i.e., number and accumulated energy) is more than 1% are selected, and the percentages of H-type and L-type waveforms, along with their energy percentages, are sorted out.

Percentages of the dominant frequency bands of AE waveform signals for dry, natural, and saturated samples are shown in Fig. 6, Fig. 7, and Fig. 8, respectively. In line with the findings of Li et al. (2017), there are two concentrations of dominant frequency bands in marble under different conditions, named the low dominant frequency band (L-type band) and high dominant frequency band (H-type band). AE waveforms located in low and high dominant frequency bands are called L-type and H-type waveforms correspondingly. It is, thus, confirmed that the feature of twin-peak in dominant frequency is intrinsic for rocks under uniaxial tension, regardless of the existence of water. All samples under uniaxial tension are dominated by L-type waveforms, along with rare H-type waveforms. In addition, the resonant frequency of the micro 30 sensors used in this study is 125 kHz. However, no aggregation phenomenon near 125 kHz in the dominant frequency of AE waveforms was observed for rock samples under different states. This finding indicates that neither the resonant frequency of the sensor nor the rock moisture condition is correlative with the dominant frequency characteristics of AE waveforms.

Figure 9 shows the distribution range of high and low dominant frequency bands of samples. The central band is defined as the largest percentage of dominant frequency within the H-type or L-type. It can be found that water has weak effects on both the range of dominant frequency bands and the central band. The amount of AE waveforms from the 2nd to 10th and 21st to 25th frequency bands constitutes almost all proportions. Compared with the central band of high dominant frequency stably located in the 24th or 25th frequency bands for all samples, this for low dominant frequency varied greatly. In particular, the low dominant frequency in the range of 20–30 kHz, 60–70 kHz, and 80–90 kHz (3rd, 7th, and 9th frequency bands) should be paid more attention to, which is L-type central bands corresponding to the failure of marble under uniaxial tension.

In Table 2, one can see that the amount of AE waveforms for dry rock is an average of 887, while those for natural and saturated rock are 1034 and 1213, respectively. Unlike the finding under uniaxial compression (Zhu et al. 2020), the AE sum increases with increasing water content. The number of L-type waveforms of dry samples accounts for 91.67% on average compared with 7.51% for H-type bands. The proportions of L-type and H-type waveforms of natural samples are 93.09% and 6.68% on average, respectively. Compared to dry and natural samples, the proportion of L-type waveforms of saturated samples released increases to 96.81% on average, whereas the proportion decreases to 2.67% for H-type waveforms. This observation supports the evidence that the percentages of L-type waveforms increase with an increase in water content, as shown in Fig. 10. Additionally, the increment of percentage in L-type waveforms for natural

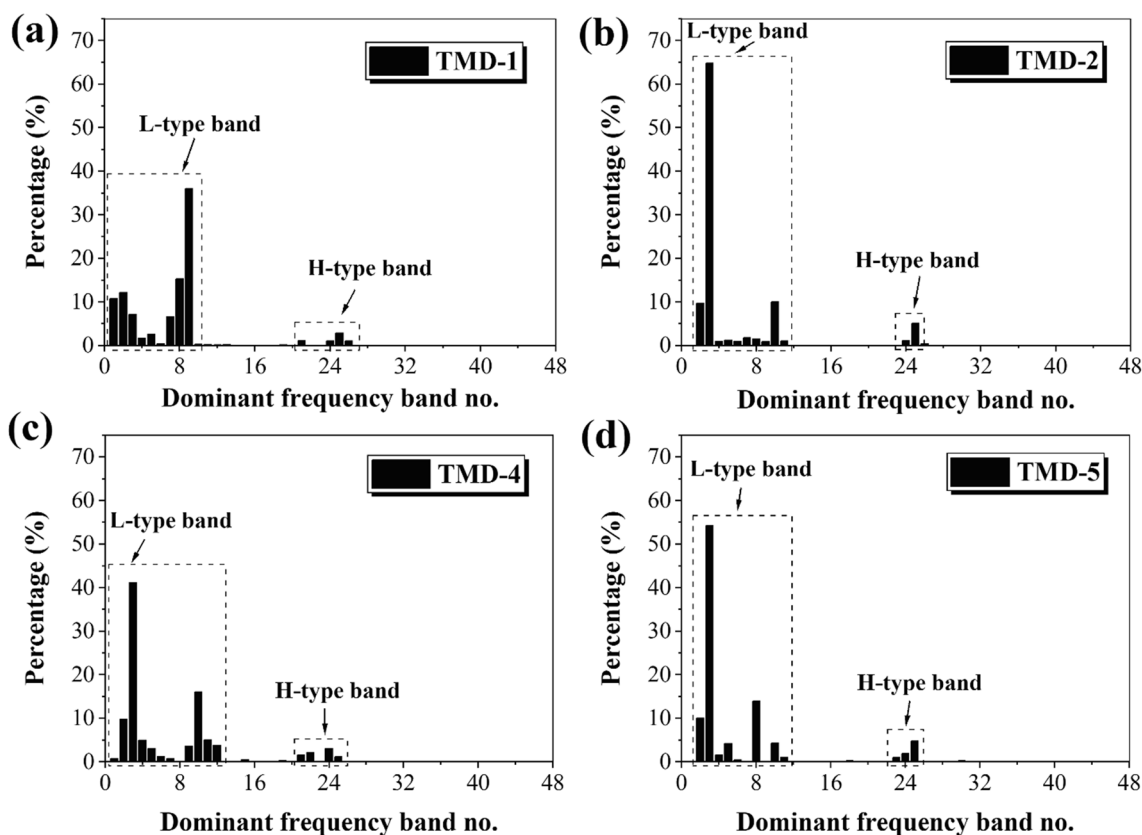


Fig. 6 Percentage of AE waveform distributed in different dominant frequency bands for dry specimens

rock is smaller than that of saturated rock. This is probably due to the less water content for natural rock as mentioned previously. There is a dramatic decrease in both cumulative energy of H-type and L-type waveforms as the water content increases. It reveals that the existence of water reduces rock brittle and the intensity of the fracture. The cumulative energy ratios of H-type and L-type waveforms of samples within a particular group show little dispersion. The minimum and maximum cumulative energy ratios of L-type waveforms for dry samples are approximately 91.29% and 96.41%, and their average value is 93.97% (Table 2). When the water content increases, the average cumulative energy ratios of L-type waveforms slightly increase to 96.20% and 99.58% for natural and saturated samples, respectively.

The cumulative percentage of H-type and L-type AE waveform signals of dry, natural, and saturated samples versus the normalized applied stress are shown in Figs. 11, 12, and 13, respectively. The normalized applied stress is defined as the ratio of the current stress (σ) to the peak stress (σ_r). Expecting the dominant role in proportion, L-type waveforms are always detected prior to H-type ones in all specimen conditions. Interestingly, the initial release time of L-type waveforms is advanced as water content increases. The initial release of L-type waveforms for dry samples

occurs at a normalized applied stress of 33.84% on average, whereas those for natural and saturated samples on the average decrease to 3.63% and 2.20%. Moreover, since the initial release of H-type waveforms generally happens after a large value of normalized applied stress (beyond 30%), the time interval of initial release between H-type and L-type waveforms becomes greater after saturation. Overall, the AE waveform signals are concentrated and released at the peak stress for all samples. The proportion of L-type AE waveforms released before peak stress for dry samples is on average 28.63%, while those for natural and saturated samples are 24.68% and 11.10%, respectively. Despite the larger data scatter of the natural group, it indicates that the proportion of L-type waveforms observed before peak stress decreases as the water content increases. In other words, more L-type waveforms are likely to be released after reaching peak stress due to the existence of water.

Relationship between failure patterns and dominant frequency of AE waveform

Here we utilized a series of AE parameters, including AE counts N , duration time T_d , rise time T_r , and maximum amplitude A_m , to identify the modes of cracks generated. To

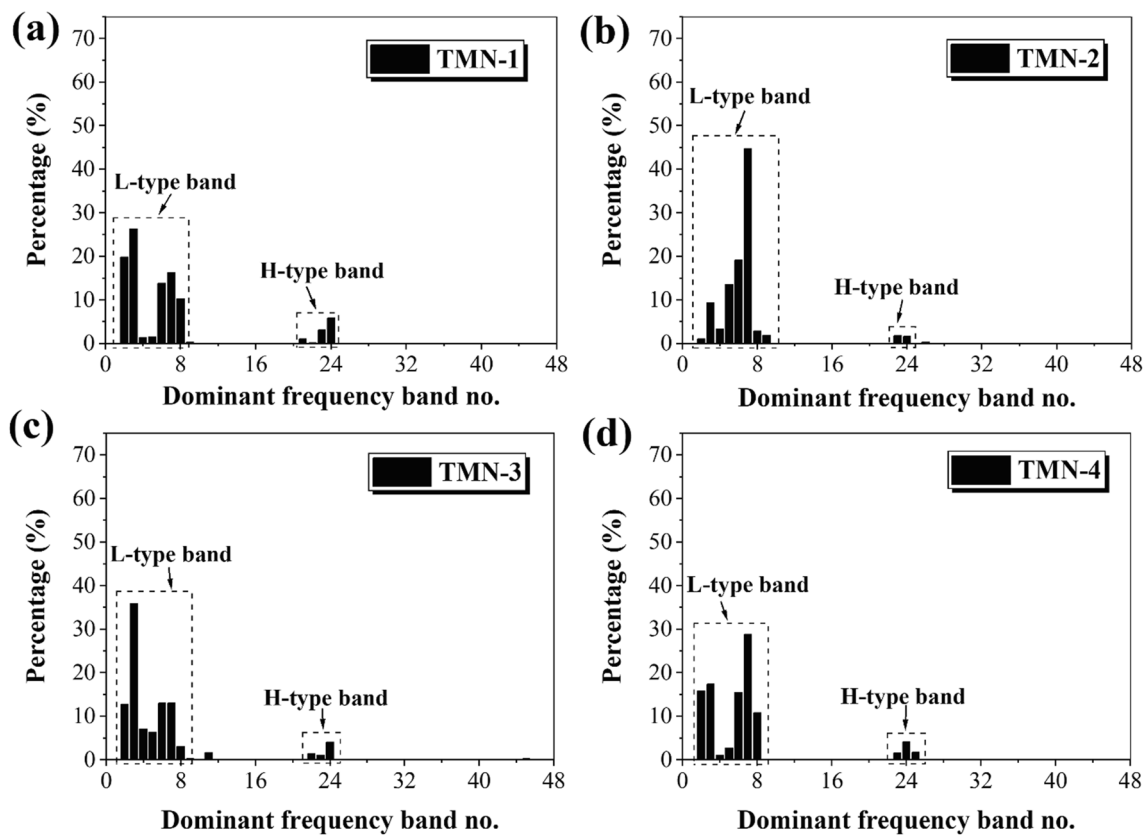


Fig. 7 Percentage of AE waveform distributed in different dominant frequency bands for natural specimens

be specific, two important parameters, the RA value and the average frequency (AF) namely, of AE signals are calculated by the following equations:

$$RA = \frac{T_r}{A_m} \quad (3)$$

$$AF = \frac{N}{T_d} \quad (4)$$

It is widely known that AE signals with a low RA value but a high AF value induce by the propagation of cracks in the tensile mode, and AE signals with a high RA value but a low AF value result from the propagation of cracks in the shear mode (Aggelis et al. 2011; Wang et al. 2017). Furthermore, the amount of these two types of cracks can be determined by a transition line, whose slope is defined as the ratio of the AF and RA values. Since the ratio of the AF and RA values k is found to vary with materials and experimental conditions, three optimal k of dry, natural, and saturated rocks under uniaxial tension were proposed in our previous publication (Zhu et al. 2022). In this study, we adopted the previous results of crack classification derived from the AE parameter method to compare with the results

of the dominant frequency of AE waveforms. As shown in Fig. 14, a good corresponding relationship between the dominant frequency of the AE waveform and failure patterns of rocks under different conditions can be observed, that is, the percentages of H-type waveforms and shear failures are almost equivalent, and so the same with the percentages of L-type waveforms and tensile failures. This indicates that the H-type waveforms are produced by micro-shear failure and the L-type waveforms are released by micro-tensile failure. Compared with the results of the first motion polarity method and the moment tensor method conducted by Li et al. (2017), the corresponding relationship between AE waveforms located in two dominant frequency bands and failure patterns is further verified by the AE parameters method for rock under tension.

Failure evolution characteristic of water-bearing rock under uniaxial tension

Since H-type waveform signal is caused by micro-shear failure and L-type waveform signal is released by micro-tensile failure mentioned above, the results of this study show that micro-shear and micro-tensile failure on average account for

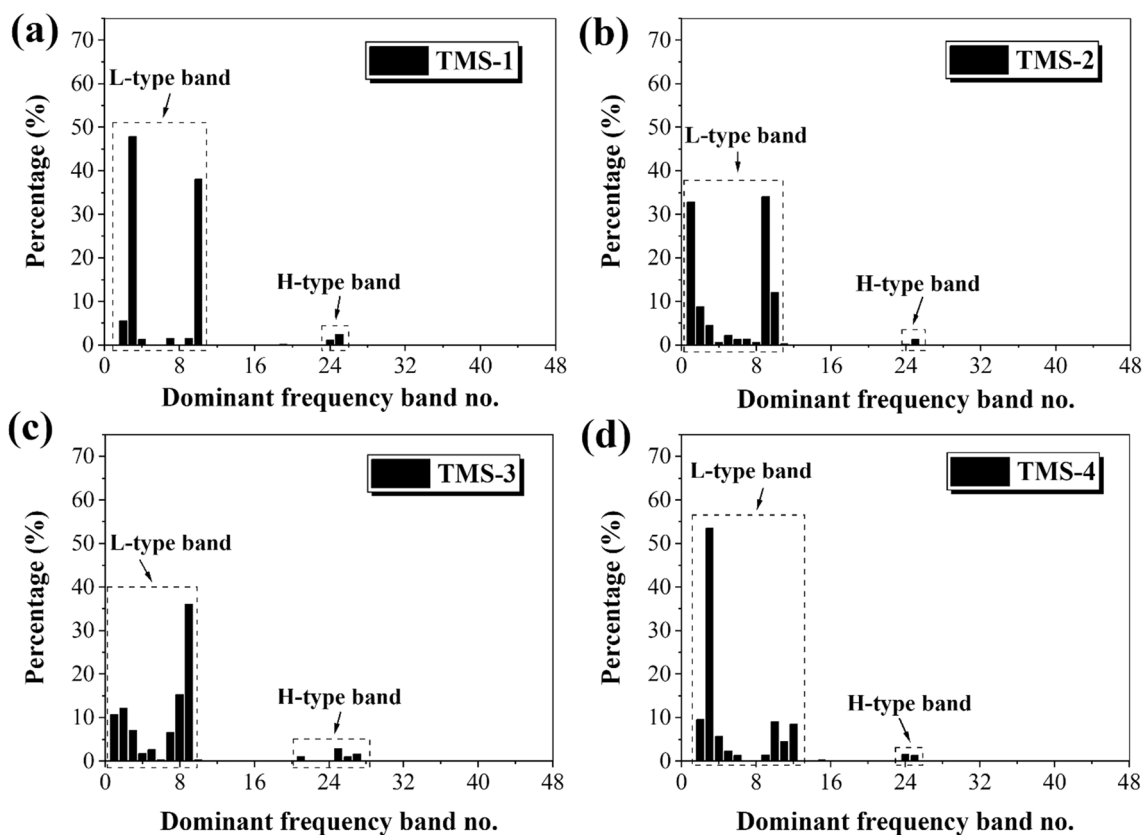


Fig. 8 Percentage of AE waveform distributed in different dominant frequency bands for saturated specimens

approximately 7.51% and 91.67%, respectively, of the total failure events during entire uniaxial tension process for dry rock. As water content increases, growing percentages of

L-type waveforms for natural (approximately 93.09%) and saturated rock (approximately 96.81%) indicate more micro-tensile failure events since their AE waveforms sum also

Fig. 9 Distribution range of high and low dominant frequency bands of rock specimens

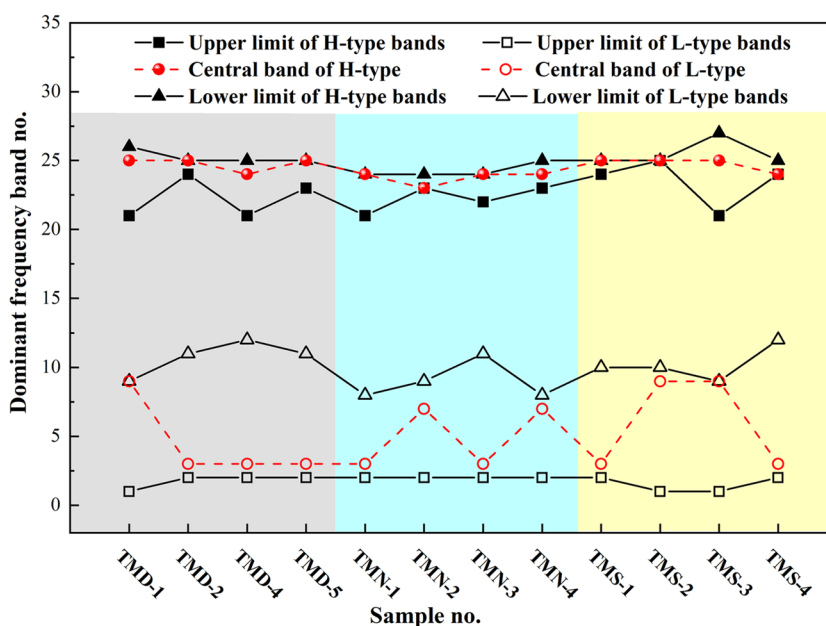


Table 2 Amount and energy ratio of L-type waveforms for rock under different conditions

Rock condition	Dry	Natural	Saturated
Average amount of AE waveforms	887	1034	1213
Minimum amount ratio of L-type waveforms (%)	90.26	89.77	95.11
Maximum amount ratio of L-type waveforms (%)	93.12	96.34	98.70
Average amount ratio of L-type waveform (%)	91.67	93.09	96.81
Minimum cumulative energy ratio of L-type waveforms (%)	91.29	94.22	99.20
Maximum cumulative energy ratio of L-type waveforms (%)	96.41	98.95	99.90
Average cumulative energy ratio of L-type waveforms (%)	93.97	96.20	99.58

grow compared with dry rock. The average energy ratio of micro-tensile failure for all samples is approximately 96.58% as opposed to 3.42% for that micro-shear failure. These observations validate that micro-tensile failures always play a dominant role and are far more abundant than micro-shear failures, which agrees with the prior studies of Li (2017) and Deng et al. (2018). Furthermore, we concluded that the dominant role of micro-tensile failure of rocks under tension is not affected by water content.

Cumulative L-type and H-type waveforms with normalized applied stress reflect the roles of micro-tensile and micro-shear failures in the macro-failure of rock. When the rock is subjected to uniaxial tension, micro-tensile failures occur before micro-shear failures and keep a major role at all loading stages. Compared with the initial release of micro-tensile failures at a normalized applied stress of 33.84% on average for dry rock, those for natural and saturated rock are 3.36 and 2.20%, respectively. The results reveal that the presence of water results in an earlier generation of micro-tensile failures. The normalized applied stress corresponding to the initial release of micro-shear failure for dry rock is 69.41% on average, whereas those for natural and saturated rock drop to 42.37 and 45.26%. This is probably attributed to the earlier generation of micro-tensile failures for the effects

of water. As reported by Wang et al. (2019), the generation of micro-shear and micro-tensile failures follows and promotes each other during tension loading. Hence, micro-tensile failures that occurred at an earlier time result in an earlier generation of micro-shear failures. Nevertheless, the time interval between the initial release of micro-shear and micro-tensile failure events becomes larger with increasing water content.

Micro-shear and micro-tensile failure events are generally concentrated and released at peak stress under uniaxial tension. The average proportion of micro-tensile failure events after reaching peak stress for dry rock is 71.37%, while those for natural and saturated rock are 75.33 and 88.90%, respectively. We found that the average amount of micro-tensile failures generated after reaching peak stress for natural and saturated rock are approximately 726 and 1045, respectively, compared to 577 for dry rock. It suggests that, as water content increases, more tensile failure events are generated after reaching peak stress. Moreover, compared with the amount of micro-shear failure events after reaching peak stress for dry rock, those for natural and saturated rock show a slight decrease.

Discussion

We documented the tensile mechanical parameters and failure progressive process of marble rock with different water contents. Overall, we find that the presence of water affects rock mechanical property and failure behavior, such as weakening the tensile strength parameters and their dispersion, advancing the initial release of micro-failures, and hosting the amount and energy of different failure components (i.e., micro-tensile failure and micro-shear failure). In this sense, we would like now to discuss the three aspects of water-bearing effects in the following.

Water-bearing effect on the dispersion of strength parameters

For the tensile strength and deformation modulus of marble, there are fewer data variations after saturation. Even though

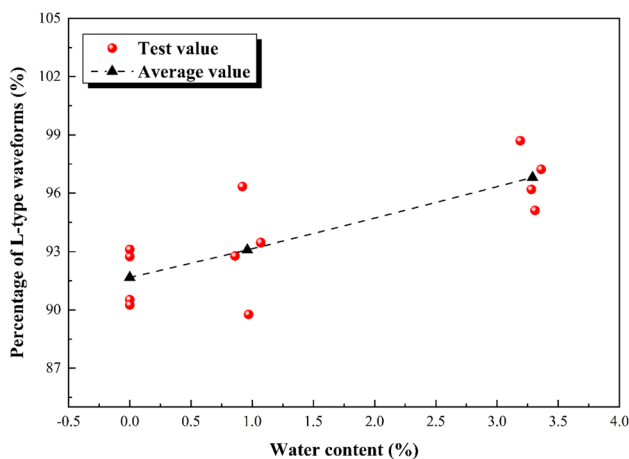


Fig. 10 Variation of the percentage of L-type waveforms versus water content

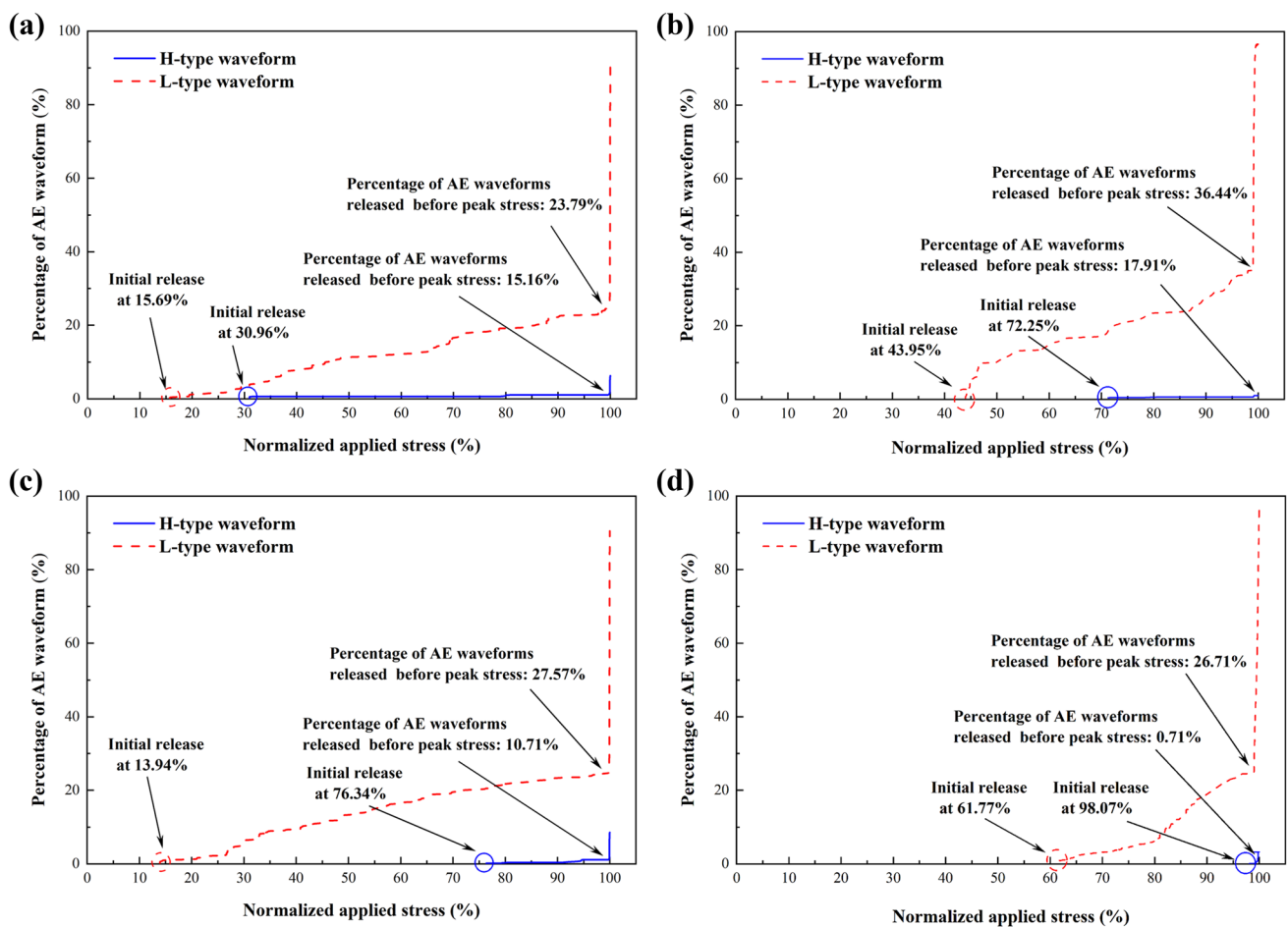


Fig. 11 Cumulative percentages of H-type and L-type AE waveforms in dry specimens with increasing normalized applied stress, **a** TMD-1, **b** TMD-2, **c** TMD-4, **d** TMD-5

the marble used in this study has a single mineral composition, the nature and distribution of original pores and cracks can vary from one specimen to another. Okubo and Fukui (1996) pointed out that tensile fracture behavior is highly susceptible to primary defects and test conditions. By proper control of test conditions, i.e., pre-crack and AE sensors with high precision, the pre-existing flaws play a dominant role in resulting in data variations of tensile strength and deformation modulus for dry and even natural specimens. In saturated specimens, the presence of water could greatly reduce the fracture intensity, which is supported by the reduction in energy of failure events of saturated rock shown in Fig. 15. The friction weakening between mineral particles caused by water is believed to be one reason for strength reduction under uniaxial tension (Van 1976). As the water-weakening effect on friction is less likely to vary much, the randomness of fracture is greatly reduced among different specimens. The consistency of the number and energy of micro-failure events that occurred for saturated specimens results in less scattered strength parameters.

Water-bearing effect on the initial release of micro-failures

Due to the presence of water, the initial release of micro-tensile failures is advanced, and the time interval of initial release between micro-tensile and micro-shear failures becomes longer. At the initial loading stage, there is almost no crack generation and propagation for dry rock, and thus AE waveform signals undergo a quiet period. Nevertheless, when the pores inside rock are full of water, the activities of micro-failure events are more likely to happen. Zhu et al. (2019) summarized four water–rock interaction mechanisms for typical rocks. For marble with single mineral composition and free of clay and siliceous minerals in this study, water-weakening effects on it are mainly friction weakening and pore water pressure. Since the condition of pores filling with water does not change and no new cracks generate at the initial loading stage, the pore water pressure is taken into account for explaining the occurrence of micro-tensile failures for saturated rock. To be specific, for those primary

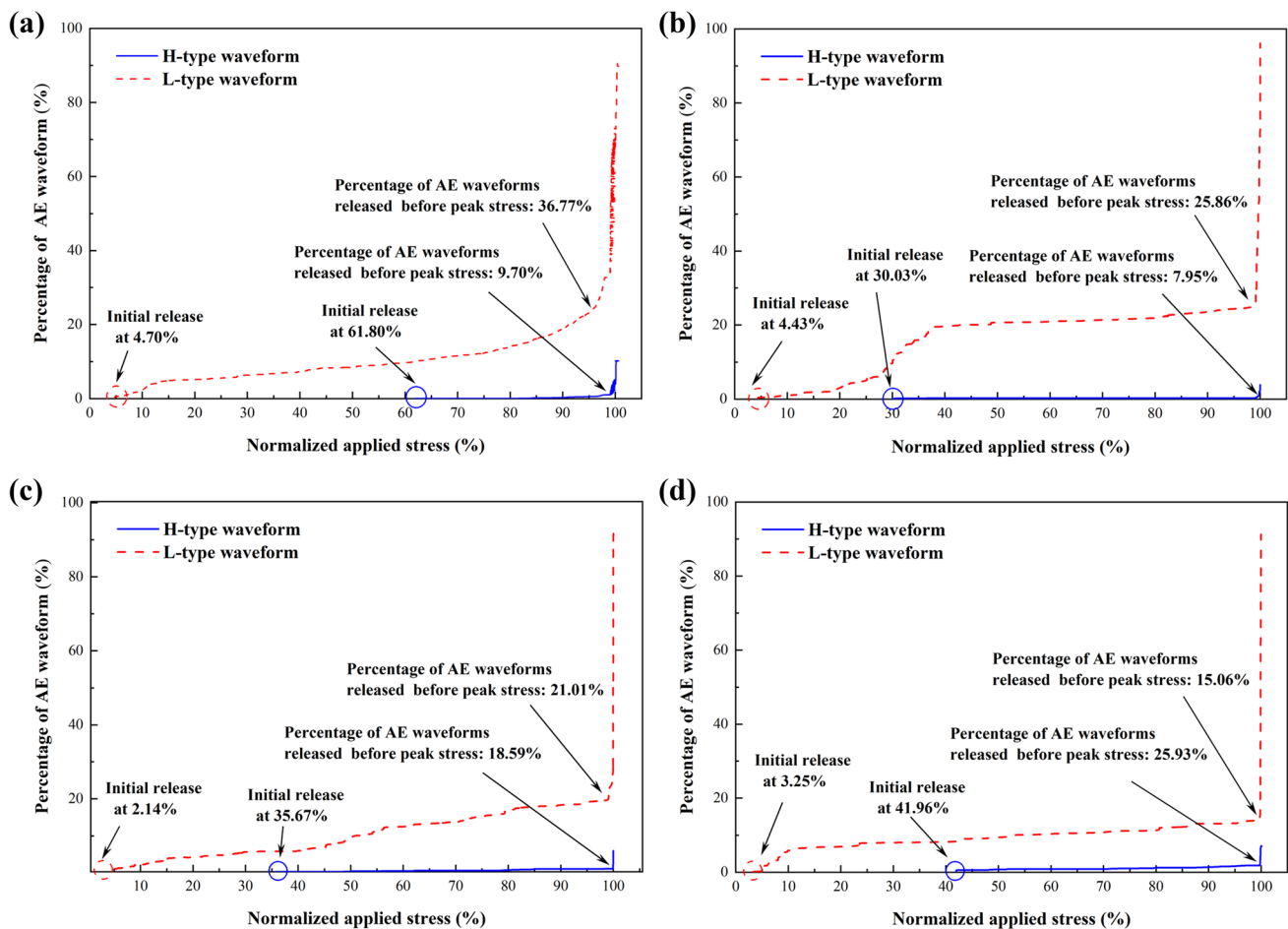


Fig. 12 Cumulative percentages of H-type and L-type AE waveforms in natural specimens with increasing normalized applied stress, **a** TMN-1, **b** TMN-2, **c** TMN-3, **d** TMN-4

pores or cracks that are not parallel to the loading direction, compress effects will exert on the water inside because of tensile loading, inducing pore water pressure. Given the formation mechanism of micro-tensile failure, the pore water pressure is very likely to be the cause of the micro-tensile failure of saturated rock at the initial loading stage.

Water-bearing effect on the rock failure behavior based on the feature of micro-shear failures

The characteristic of micro-failures, i.e., amount and energy, is essential for the analysis of rock tensile fracture behavior. As shown in Fig. 15, the increasing water content increased the amount of micro-tensile failures generally, along with a reduction in the amount of micro-shear failures. Since the ability of the brittle rock to stretch is much lower than that of compress (Goodman 1989; Wu et al. 2018), more micro-tensile failures occurred accelerate the crack propagation substantially, which results in tensile strength reduction. Furthermore, the increasing water contents make the energy

of micro-tensile failures reduce slightly, indicating that the micro-tensile failure events released are less intense due to the existence of water. In comparison, the trend of increase in the amount of micro-shear failure is more obvious than that in its energy. It is, thus, concluded that the amount of micro-tensile failures has a more dominant effect on tensile strength. Drastic loss in the energy of micro-shear failures was observed with increasing water contents. Specifically, the average energy of micro-shear failures released after peak stress for dry rock is $2.64 \times 10^3 \text{ mV}^2$, while that for saturated rock is $1.17 \times 10^2 \text{ mV}^2$, with a drop of 95.57%. This finding indicates water causes the intensity of micro-shear failures to be greatly reduced. Despite the reduction of micro-shear failure amount, the drastic loss in its energy seems largely related to the tensile strength degradation due to the existence of water.

The failure mechanism of rock subjected to uniaxial tension loading is described as the overcome of the cohesion on the cross-section. As shown in Fig. 16, the potential failure surface of the rock is rough because of its complex and

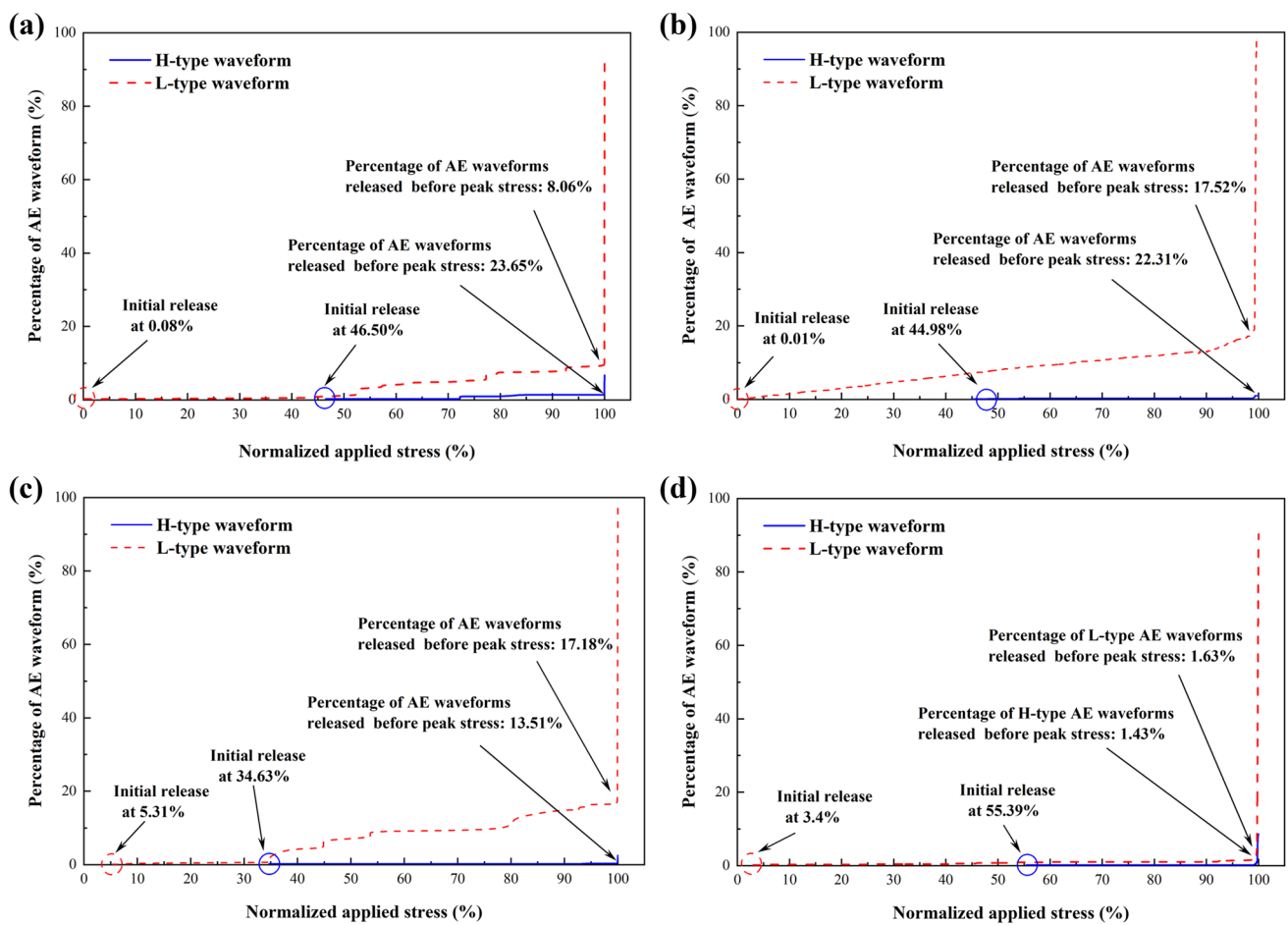


Fig. 13 Cumulative percentages of H-type and L-type AE waveforms in saturated specimens with increasing normalized applied stress, a TMS-1, b TMS-2, c TMS-3, d TMS-4

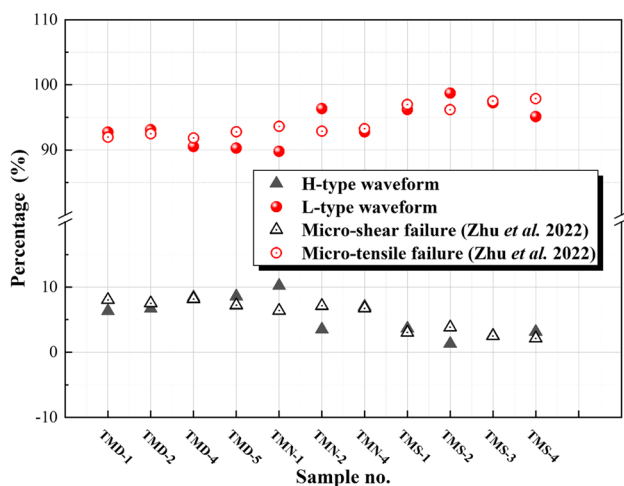


Fig. 14 Corresponding relationship between dominant frequency of the waveform and micro-failure types

irregular arrangement of mineral particles. The frictional force thus arises when tensile force was applied. Moreover, the tendency or occurrence of crystal particle slip occurring in original defect planes which are not perpendicular to the loading direction is also responsible for the frictional force. The net force of frictional force f and bond force F_c is in equilibrium with the tensile force T_1 . During rock saturation, the lubricating water films are formed in their original pores and cracks because of the adsorption of water molecules. These water films would undoubtedly reduce the friction present in the original pores and cracks, as well as in the potential failure surfaces. The frictional force f , as would be expected, decreased. Note that the friction between mineral particles is believed to be the reason for micro-shear failure. In this connection, it should be recalled that the energy of micro-shear failures after peak stress is reduced significantly, which supports the existence of friction weakening due to the water films. In other words, even though micro-tensile failures play a dominant role in rock tensile fracture, the reduction in amount, especially in energy, of micro-shear

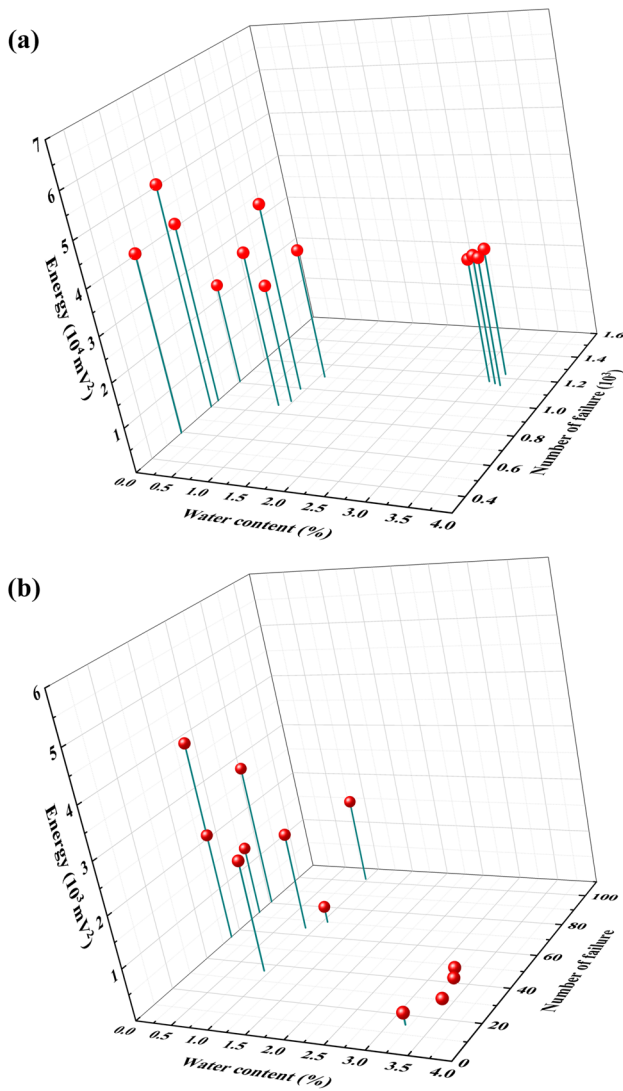


Fig. 15 Relationship between different types of micro-failure and water content, **a** micro-tensile failure, **b** micro-shear failure

failures can be largely responsible for the strength loss of rock under moisture states. This seems to overturn the traditional understanding and emphasis the important synergistic role of micro-shear failure in water-bearing rock fracture under tension loading.

Here we explore the correlation between the energy and energy ratio of micro-shear failures (E_s and P_{E_s}) with the tensile strength of rock samples. The relationships between E_s , P_{E_s} and σ_t were modeled by using the linear function, as shown in Fig. 17. The slopes of the two fitting lines were 32.53 and 7.77, respectively, and suggested an apparent positive correlation between the energy and energy ratio of micro-shear failures with tensile strength. As we know, when rock is in a less moisture environment, more micro-shear failure events with high energy are activated, which is believed to result from the friction generated during tension

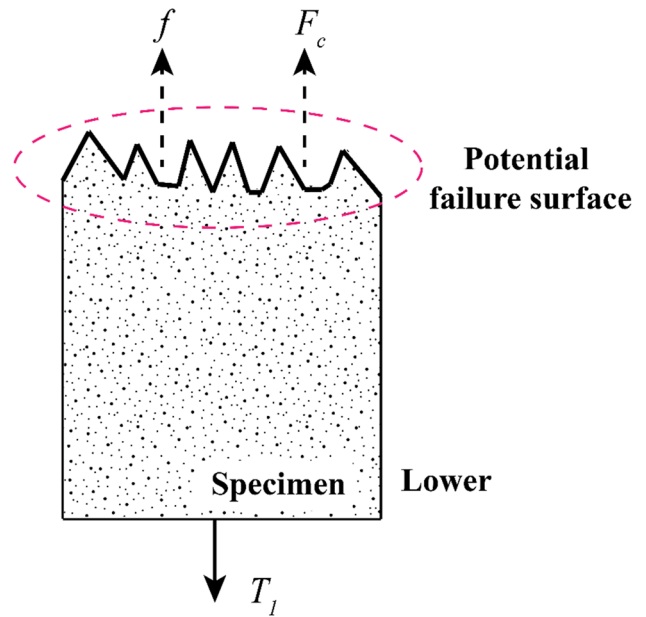


Fig. 16 Diagram of rock forces under uniaxial tension

loading. The tensile strength increases as a result of the strong friction effect. In turn, the weak friction induced by water could lead to a reduction in energy of micro-shear failure and further cause tensile strength loss. Another piece of evidence is the scanning electron microscope (SEM) images detected on the fracture surfaces of dry and saturated rocks. Figure 18 depicts that several trans-granular fractures are observed in the failure process of dry rock when locally magnified to a large enough time. The surfaces of these trans-granular fractures are smooth, indicating violent rupture patterns with high energy. The fracture with a smooth

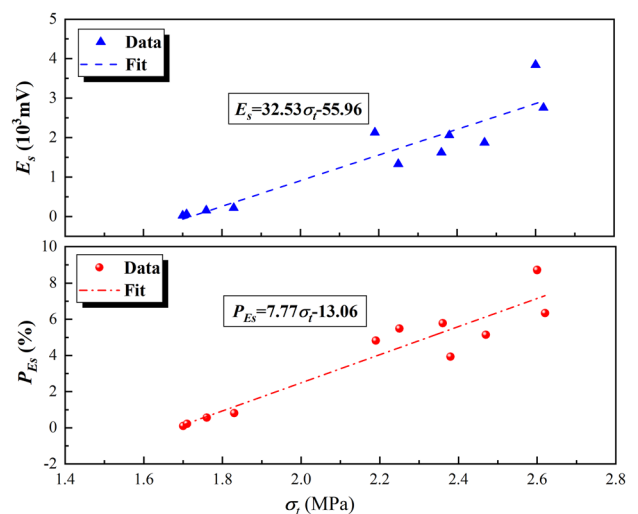


Fig. 17 Correlation of energy and energy ratio of micro-shear failures (E_s and P_{E_s}) with tensile strength

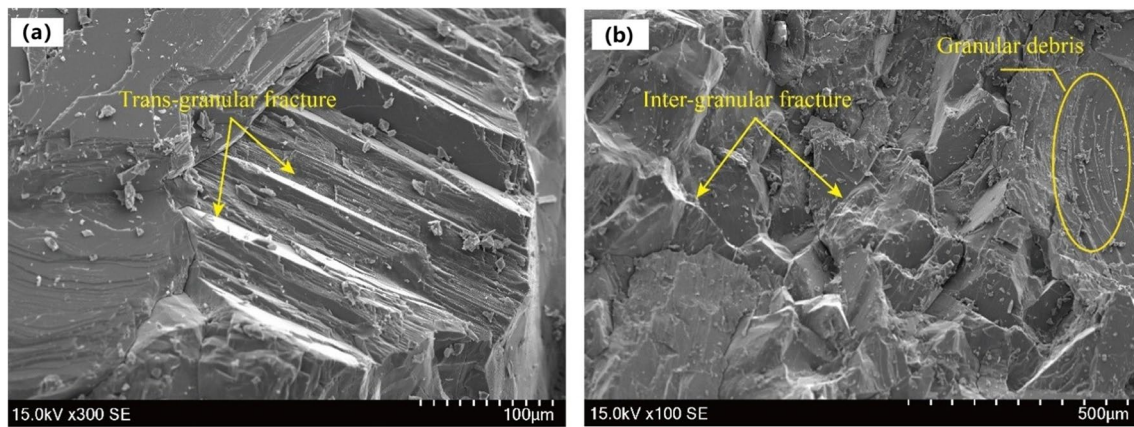


Fig. 18 SEM images of rock samples after uniaxial tension tests, **a** dry specimen, **b** saturated specimen

surface is commonly considered to be the result of micro-shear failure induced by friction. In comparison, numerous intergranular fractures exist in the failure process of saturated rock from a relative whole view, which is manifested by uneven surfaces with flat blunt angulars. Moreover, many pieces of crystal debris were attached to the mineral surface of the saturated rock. These findings suggest that water affects the fracture patterns largely and reduces the severity of the failure events. In this sense, the drastic loss in energy and energy ratio of micro-shear failures found in this study could thus be an important reason for the strength degradation of water-bearing rock under tension.

Conclusions

The most relevant findings derived from this study are shown below:

- (1). As water content increases, the tensile strength of rock decreases significantly, while a weak trend of deformation modulus is exhibited. There are two concentrations of dominant frequency bands for rock under uniaxial tension, regardless of water content. The dominant L-type waveforms are generated before H-type waveforms under different water contents, and their percentages slightly increase with increasing water contents.
- (2). The H-type waveforms are produced by micro-shear failures, and the L-type waveforms are released by micro-tensile failures. Due to the existence of water, the initial release of micro-tensile failures is advanced, which is responsible for the weak effect of pore water pressure. The time interval of initial release between micro-tensile and micro-shear failures becomes longer.
- (3). With increasing water content, the amount of micro-tensile failures released increases, while its energy decreases. The amount and energy of micro-shear failure both reduce significantly. The mechanism involved in the drastic tensile strength reductions of water-bearing marble rock is likely to be friction weakening. The friction weakening is exerted by the water films attached to original defects and potential failure surfaces.

Funding This research was supported by the Sichuan Science and Technology Program (Grant No. 2023NSFSC0786), the National Natural Science Foundation of China (Grant No. U19A2098), and the National Key Research and Development Program of China (Grant No. 2018YFC1505004).

Data availability All data or models that support the findings of this study are available from the corresponding author upon reasonable request.

Declarations

Competing interest The authors declare no competing interests.

References

- Aggelis D, Kordatos E, Matikas T (2011) Acoustic emission for fatigue damage characterization in metal plates. *Mech Res Commun* 38(2):106–110
- Aker E, Kühn D, Vavryčuk V, Soldal M, Oye V (2014) Experimental investigation of acoustic emissions and their moment tensors in rock during failure. *Int J Rock Mech Min Sci* 70:286–295
- Calabrese L, Campanella G, Proverbio E (2013) Identification of corrosion mechanisms by univariate and multivariate statistical analysis during long term acoustic emission monitoring on a pre-stressed concrete beam. *Corros Sci* 73(aug.):161–171
- Chugh YP, Hardy HR, Stefanko R (1968) Investigation of the frequency spectra of microseismic activity in rock under tension,

- in* Proceedings The 10th US Symposium on Rock Mechanics (USRMS)OnePetro
- Deng J, Li L, Chen F, Yu J, Liu J (2018) Twin-peak frequencies of acoustic emission due to the fracture of marble and their possible mechanism. *Advanced Engineering Sciences* 50(5):12–17
- Eberhardt E, Stead D, Stimpson B, Read R (1998) Identifying crack initiation and propagation thresholds in brittle rock. *Can Geotech J* 35(2):222–233
- Goodman R (1989) *Introduction to rock mechanics*, 2nd edn. Wiley, New York
- Gunsallus K, Kulhawy F (1984) A comparative evaluation of rock strength measures. *Int J Rock Mech Min Sci Geomech Abstr* 21(5):233–248
- Hashiba K, Fukui K (2015) Effect of water on the deformation and failure of rock in uniaxial tension. *Rock Mech Rock Eng* 48(5):1751–1761
- Hawkes I, Mellor M, Garipey S (1973) Deformation of rocks under uniaxial tension. *Proc Int J Rock Mech Min Sci Geomech Abstr* 10:493–507
- He M, Miao J, Feng J (2010) Rock burst process of limestone and its acoustic emission characteristics under true-triaxial unloading conditions. *Int J Rock Mech Min Sci* 47(2):286–298
- Hobbs D (1967) Rock tensile strength and its relationship to a number of alternative measures of rock strength. *Int J Rock Mech Min Sci Geomech Abstr* 4(1):115–127
- Kim E, Stine M, Oliveira D, Changani H (2017) Correlations between the physical and mechanical properties of sandstones with changes of water content and loading rates. *Int J Rock Mech Min Sci* 100:255–262
- Lajtai E (1980) Tensile strength and its anisotropy measured by point and line-loading of sandstone. *Eng Geol* 15(3–4):163–171
- Li L (2017) Dominant frequencies and their mechanical mechanism of acoustic emissions in rock failures. Sichuan University, Chengdu
- Li L, Deng J, Zheng L, Liu J (2017) Dominant frequency characteristics of acoustic emissions in white marble during direct tensile tests. *Rock Mech Rock Eng* 50(5):1337–1346
- Li H, Shen R, Wang E, Li D, Li T, Chen T, Hou Z (2020) Effect of water on the time-frequency characteristics of electromagnetic radiation during sandstone deformation and fracturing. *Eng Geol* 265:105451
- Liao Z, Zhu J, Tang C (2019) Numerical investigation of rock tensile strength determined by direct tension, Brazilian and three-point bending tests. *Int J Rock Mech Min Sci* 115:21–32
- Liu J, Chen L, Wang C, Man K, Wang L, Wang J, Su R (2014) Characterizing the mechanical tensile behavior of Beishan granite with different experimental methods. *Int J Rock Mech Min Sci* 69(3):50–58
- Liu J, Li Y, Xu S, Xu S, Jin C (2015) Cracking mechanisms in granite rocks subjected to uniaxial compression by moment tensor analysis of acoustic emission. *Theoret Appl Fract Mech* 75:151–159
- Liu H, Zhu W, Yu Y, Xu T, Li R, Liu X (2020) Effect of water imbibition on uniaxial compression strength of sandstone. *Int J Rock Mech Min Sci* 127:104200
- Lockner D (1993) The role of acoustic emission in the study of rock fracture. *Int J Rock Mech Min Sci Geomech Abstr* 30(7):883–899
- Ohnaka M, Mogi K (1982) Frequency characteristics of acoustic emission in rocks under uniaxial compression and its relation to the fracturing process to failure. *J Geophys Res: Solid Earth* 87(B5):3873–3884
- Ohtsu M (1991) Simplified moment tensor analysis and unified decomposition of acoustic emission source: application to in situ hydrofracturing test. *J Geophys Res: Solid Earth* 96(B4):6211–6221
- Ohtsu M, Okamoto T, Yuyama S (1998) Moment tensor analysis of acoustic emission for cracking mechanisms in concrete. *Struct J* 95(2):87–95
- Ojo O, Brook N (1990) The effect of moisture on some mechanical properties of rock. *Min Sci Technol* 10(2):145–156
- Okubo S, Fukui K (1996) Complete stress-strain curves for various rock types in uniaxial tension. *Int J Rock Mech and Min Sci Geomech Abstr* 33(6):549–556
- Perras MA, Diederichs MS (2014) A review of the tensile strength of rock: concepts and testing. *Geotech Geol Eng* 32(2):525–546
- Rabat Á, Tomás R, Cano M (2020) Evaluation of mechanical weakening of calcarenite building stones due to environmental relative humidity using the vapour equilibrium technique. *Eng Geol* 278:105849
- Shakoor A, Barefield E (2009) Relationship between unconfined compressive strength and degree of saturation for selected sandstones. *Environ Eng Geosci* 15(1):29–40
- Shiotani T, Ohtsu M, Ikeda K (2001) Detection and evaluation of AE waves due to rock deformation. *Constr Build Mater* 15(5):235–246
- Stimpson B, Chen R (1993) Measurement of rock elastic moduli in tension and in compression and its practical significance. *Can Geotech J* 30(2):338–347
- Sun X, Xu H, Zheng L, He M, Gong W (2016) An experimental investigation on acoustic emission characteristics of sandstone rockburst with different moisture contents. *Sci China Technol Sci* 59(10):1549–1558
- Talesnick M, Hatzor YH, Tsesarsky M (2001) The elastic deformability and strength of a high porosity, anisotropic chalk. *Int J Rock Mech Min Sci* 38(4):543–555
- Ulusay R (2015) *The ISRM suggested methods for rock characterization, testing and monitoring: 2007–2014*. Springer Cham
- Van E (1976) The mechanisms of strength reduction due to moisture in coal mine shales. *Int J Rock Mech Min Sci Geomech Abstr* 13(2):61–67
- Verstrynghe E, Adriaens R, Elsen J, Van Balen K (2014) Multi-scale analysis on the influence of moisture on the mechanical behavior of ferruginous sandstone. *Constr Build Mater* 54:78–90
- Vishal V, Ranjith P, Singh TN (2015) An experimental investigation on behaviour of coal under fluid saturation, using acoustic emission. *J Nat Gas Sci Eng* 22:428–436
- Wang M, Tan C, Meng J, Yang B, Li Y (2017) Crack classification and evolution in anisotropic shale during cyclic loading tests by acoustic emission. *J Geophys Eng* 14(4):930–938
- Wang W, Yao Q, Tang C, Li X, Chong Z, Xu Q (2021) Experimental study on the shear characteristics and weakening mechanism of water-bearing rock joints. *Bull Eng Geol Env* 80(10):7653–7668
- Wang Y, Deng J, Li L, Zhang Z (2019) Micro-failure analysis of direct and flat loading Brazilian tensile tests. *Rock Mech Rock Eng* 52(11):4175–4187
- Wong LNY, Jong MC (2014) Water saturation effects on the Brazilian tensile strength of gypsum and assessment of cracking processes using high-speed video. *Rock Mech Rock Eng* 47(4):1103–1115
- Wu C, Chen X, Hong Y, Xu R, Yu D (2018) Experimental investigation of the tensile behavior of rock with fully grouted bolts by the direct tensile test. *Rock Mech Rock Eng* 51(1):351–357
- Yao Q, Chen T, Ju M, Liang S, Liu Y, Li X (2016) Effects of water intrusion on mechanical properties of and crack propagation in coal. *Rock Mech Rock Eng* 49(12):4699–4709
- Zang A, Christian F, Stanchits S, Dresen G, Andresen R, Haidekker M (1998) Source analysis of acoustic emissions in Aue granite cores under symmetric and asymmetric compressive loads. *Geophys J Int* 135(3):1113–1130
- Zhang Y, Liang P, Liu X, Liu S, Tian B (2015) Experimental study on precursor of rock burst based on acoustic emission signal dominant -frequency and entropy. *Chin J Rock Mech Eng* 34:2959–2967

- Zhang Z, Deng J, Zhu J, Li L (2018) An experimental investigation of the failure mechanisms of jointed and intact marble under compression based on quantitative analysis of acoustic emission waveforms. *Rock Mech Rock Eng* 51(7):2299–2307
- Zhang Z, Deng J (2020) A new method for determining the crack classification criterion in acoustic emission parameter analysis. *Int J Rock Mech Min Sci* 130
- Zhao K, Yang D, Zeng P, Huang Z, Wu W, Li B, Teng T (2021) Effect of water content on the failure pattern and acoustic emission characteristics of red sandstone. *Int J Rock Mech Min Sci* 142:104709
- Zhu J, Deng J, Chen F, Huang Y, Yu Z (2020) Water saturation effects on mechanical and fracture behavior of marble. *Int J Geomech* 20(10):04020191. [https://doi.org/10.1061/\(ASCE\)GM.1943-5622.0001825](https://doi.org/10.1061/(ASCE)GM.1943-5622.0001825)
- Zhu J, Deng J, Chen F, Wang F (2022) Failure analysis of water-bearing rock under direct tension using acoustic emission. *Eng Geol* 299:106541
- Zhu J, Deng J, Huang Y, Yu Z (2019) Experimental study on characteristic strength of saturated marble. *Chin J Rock Mech Eng* 38(6):1129–1138

Springer Nature or its licensor (e.g. a society or other partner) holds exclusive rights to this article under a publishing agreement with the author(s) or other rightsholder(s); author self-archiving of the accepted manuscript version of this article is solely governed by the terms of such publishing agreement and applicable law.